 CMES, vol.72, no.2, pp.115-147, 2011

A Fast Multipole Dual Boundary Element Method for the Three-dimensional Crack Problems

H. T. Wang[1,2] and Z. H. Yao[3]

Abstract: A fast boundary element solver for the analysis of three-dimensional general crack problems is presented. In order to effectively model the embedded or edge cracked structures a dual boundary integral equation (BIE) formulation is used. By implementing the fast multipole method (FMM) to the discretized BIE, structures containing a large number of three-dimensional cracks can be readily simulated on one personal computer. In the FMM framework, a multipole expansion formulation is derived for the hyper-singular integral in order that the multipole moments of the dual BIEs containing the weakly-, strongly- and hyper-singular kernels are collected and translated with a unified form. In the numerical examples, the accuracy of the proposed method for the evaluations of both the crack opening displacement (COD) and stress intensity factor (SIF) is tested, and its performance in both the memory consumption and solution time in comparison with several other algorithms is investigated. The results are shown to demonstrate the effectiveness of this method for large-scale crack problems.

Keywords: dual boundary element method, fast multipole, large-scale, crack opening displacement, stress intensity factor

1 Introduction

The main attractive feature of the boundary element method (BEM) for the analysis of linear elastic fracture mechanics (LEFM) is that only the boundary of the analyzed domain needs to be discretized (Cruse 1996). This results not only in the simplification of the crack meshing process, but also in a reduction of the degrees of freedom with respect to other numerical methods. In addition, the BEM provides an efficient way to deal with the inherent nature of singularity at the crack tip

[1] Corresponding author. Tel.: + 86 10 6278 4824; fax: + 86 10 6279 7136. Email address: wanght@tsinghua.edu.cn (H. Wang)
[2] Institute of Nuclear & New Energy Technology, Tsinghua University, Beijing, 100084, P. R. China
[3] School of Aerospace, Tsinghua University, Beijing, 100084, P. R. China

via special treatments on only the crack tip boundary elements. Direct application of the displacement BEM to crack problems leads to a degenerated system matrix when two crack surfaces coincide. To overcome this mathematical difficulty, several techniques have been developed in the last several decades, including the crack Green's function method (Snyder and Cruse 1975), the displacement discontinuity method (Weaver 1977) and the multi-region method (Blandford, Ingraffea and Liggett 1981). The dual boundary element method (DBEM) is a novel technique that provides a single-region formulation for the analysis of general crack problems. The DBEM was first introduced for the analysis of two-dimensional crack problems by Portela and Aliabadi (1992) and three-dimensional crack problems by Mi and Aliabadi (1992). This technique was then extensively studied and successfully applied to a wide range of fracture mechanics problems (Portela, Aliabadi and Rooke 1993, Mi and Aliabadi 1994, Chen and Chen 1995, Salgado and Aliabadi 1996, Young 1996, Aliabadi 1997, Cisilino and Aliabadi 1997 and 2004, Chen, Chen, Yeih and Shieh 1998, Wilde and Aliabadi 1999, Partheymüller, Haas and Kuhn 2000, Burczynski and Beluch 2001, Chao, Chen and Lin 2001, Albuquerque, Sollero and Aliabadi 2004, Purbolaksono and Aliabadi 2005, Kebir, Roelandt and Chambon 2006).

Conventionally, the system matrix denoted by $[\mathbf{A}]$ arising from the BEM is fully-populated. This feature poses a serious challenge to the BEM since to solve the equation system $[\mathbf{A}]\{\mathbf{X}\} = \{\mathbf{B}\}$ by use of standard direct or iterative solvers, a computational cost of $O(N^3)$ or $O(N^2)$ is required, where N is the number of unknowns. In order to improve the efficiency of the BEM, much effort has been devoted to the implementation of fast algorithms to the BEM solutions. Of particular interest was the fast multipole method (FMM) originally proposed by Rokhlin (1985) for classical potential theory. The FMM has been successfully extended for the fast BEM solutions for large-scale problems in the area of elasticity (Fu, Klimkowski, Rodin and colleagues 1998, Popov and Power 2001, Takahashi, Nishimura and Kobayashi 2003, Liu, Nishimura, Otani and colleagues 2005, Wang and Yao 2005, Liu 2006, Sanz, Bonnet and Dominguez 2008, Wang, Hall, Yu and Yao 2008, Wang and Yao 2008). A comprehensive review can be found in the literature (Nishimura 2002).

For the fast multipole BEM solutions of crack problems, we categorize recent investigations into two groups according to the dimensional cases. One group consists of researches concerning two-dimensional cracks. Helsing (1999) and Helsing and Jonsson (2002) used the FMM accelerated BEM to treat two-dimensional many elastic cracks and demonstrated the efficiency of the proposed algorithms in large scales. Englund (2006) combined the FMM and a modified integral equation formulation to compute accurately the stress field in a two-dimensional finite edge-cracked domain. Liu (2008) developed a new fast multipole formulation for the hy-

persingular BIE in conjunction with the DBEM to deal with two-dimensional multi-domain elastostatic problems with inclusions and cracks. In his study, the crack is discretized with piecewise constant boundary elements. Wang and Yao (2006) proposed a fast multipole DBEM formulation and a special crack-tip element for the two-dimensional general fatigue crack growth problems. Another group of papers contribute to the fast BEM solutions of three-dimensional crack problems. Nishimura, Yoshida and Kobayashi (1999) proposed a FM-BEM based on the efficient solid harmonic expansion formulation of the hypersingular kernels to solve three-dimensional many crack problems in an infinite domain for the Laplace equation using piecewise constant elements. Then Yoshida, Nishimura and Kobayashi (2001) applied the FMM-accelerated Galerkin BEM to three-dimensional elastic crack problems in an infinite domain using piecewise linear elements. Lai and Rodin (2003) developed a FM-BEM in conjunction with a weakly singular kernel to solve three-dimensional many crack problems in an infinite domain. In their work, the quadratic elements are used in order to get better results in comparison with linear or constant elements.

In addition to the FMM, another fast algorithm increasingly used recently for elastic crack problems is the Adaptive Cross Approximation method (ACA) proposed by Bebendorf and Rjasanow (2003). The ACA is an algebraic method whose approximation is based only on the knowledge of indivisual matrix entries. This kernel-independent feature makes it possible for the ACA to be developed as a black-box fast BEM solver. Researches on the ACA-accerelated DBEM for three-dimensionl general elastic crack problems have been reported by Kolk, Weber and Kuhn's group (Kolk, Weber and Kuhn 2005, Kolk and Kuhn 2006, Weber, Kolk and Kuhn 2009) and Aliabadi's group (Benedetti, Aliabadi and Davì 2008, Benedetti, Milazzo and Aliabadi 2009, Benedetti and Aliabadi 2010). It was shown in the literature (Buchau, Rucker, Rain and colleagues 2003, Brancati, Aliabadi and Benedetti 2009, Brunner, Junge, Rapp and colleagues 2010) that the ACA, especially the partially-pivoted ACA, has better efficiency in computational speed than the FMM. However, in contrast with the frequent report that the fast multipole BEM is capable for large-scale problems with several hundred thousand and even millions of unknowns, there is little report on the application of the ACA-accelerated BEM for the modeling of more than 100,000 unknowns. The major reason behind this is that the cost of storing the whole ACA matrix is approximately $O(N\log N)$ (Bebendorf and Rjasanow 2003), which makes ACA less efficient in storage than the FMM when N reaches up to a large value. The fast multipole BEM solver is considered to be competitive for the modeling of large and complex cracked structures whose scale beyond ACA's ability. To the best of the knowledge of the authors no application of the FMM in conjunction with the DBEM to three-dimensional general crack

problems is reported in the literature.

In this paper, a fast multipole DBEM for the analysis of three-dimensional general crack problems is presented. First, the basic idea of the DBEM for the three-dimensional linear elastic fracture mechanics is briefly reviewed and special treatments on both the element types and the nature of stress singularity at crack fronts are discussed. Next major features of the fast multipole DBEM in three-dimensions are illustrated, highlighting a multipole expansion formulation derived for the hyper-singular integral in order that the multipole moments of the dual BIEs containing the weakly-, strongly- and hyper-singular kernels are collected and translated in a unified way. The numerical examples demonstrate both the accuracy and efficiency of the proposed method.

2 Dual Boundary Element Method for Three-dimensional Fracture Mechanics

The model of an elastic structure containing several edge and embedded cracks is shown in Fig. 1. Let V and S_0 denote the domain and boundary of the elastic solid, respectively; S_C^+ and S_C^- the two coincide surfaces of the cracks.

The dual boundary integral equations (DBIEs) for three-dimensional elastic fracture mechanics without body force are expressed as (Mi and Aliabadi 1992, Cisilino

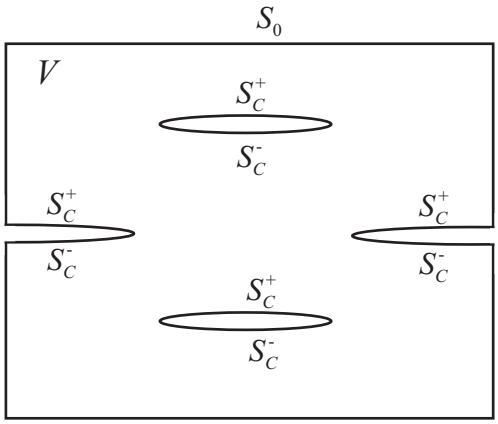

Figure 1: Model of an elastic solid containing edge and embedded cracks

and Aliabadi 1997),

$$\begin{aligned} &c_{ij}(x)\,u_j(x)+\int_{S_0}\left[T^*_{ij}(x,y)\,u_j(y)-U^*_{ij}(x,y)\,t_j(y)\right]dS(y)\\ &=-\int_{S_C^+}T^*_{ij}(x,y)\,\Delta u_j(y)\,dS(y)\ \ (x\in S_0) \end{aligned} \tag{1a}$$

$$\begin{aligned} &\frac{1}{2}\left[u_i^+(x)+u_i^-(x)\right]+\int_{S_0}\left[T^*_{ij}(x,y)\,u_j(y)-U^*_{ij}(x,y)\,t_j(y)\right]dS(y)\\ &=-\int_{S_C^+}T^*_{ij}(x,y)\,\Delta u_j(y)\,dS(y),\ \ \left(x\in S_C^-\right) \end{aligned} \tag{1b}$$

$$\begin{aligned} &\frac{1}{2}\left[t_i^+(x)-t_i^-(x)\right]+\int_{S_0}\left[S^*_{ij}(x,y)\,u_j(y)-D^*_{ij}(x,y)\,t_j(y)\right]dS(y)\\ &=-\int_{S_C^+}S^*_{ij}(x,y)\,\Delta u_j(y)\,dS(y),\ \ \left(x\in S_C^+\right) \end{aligned} \tag{1c}$$

where x and y denote the source and field points, respectively; u_i and $t_i (i=1,2,3)$ are the boundary displacement and traction vectors respectively; $c_{ij}(x)$ is a free term related to the shape of the boundary at point x; $\Delta u_i = u_i^+ - u_i^-$ is the relative displacement between S_C^+ and S_C^-; $U^*_{ij}(x,y)$ and $T^*_{ij}(x,y)$ are the kernel functions of 3-D elasticity defined as,

$$U^*_{ij}(x,y)=\frac{1}{16\pi G(1-\nu)r}\left[(3-4\nu)\delta_{ij}+r_{,i}r_{,j}\right] \tag{2a}$$

$$T^*_{ij}(x,y)=\frac{1}{8\pi(1-\nu)r^2}\left\{(1-2\nu)\left(r_{,j}n_i-r_{,i}n_j\right)-\frac{\partial r}{\partial n}\left[(1-2\nu)\delta_{ij}+3r_{,i}r_{,j}\right]\right\} \tag{2b}$$

with r denoting the distance of x and y, and G, ν being the shear modulus and Poisson's ratio, respectively. $D^*_{ij}(x,y)$ and $S^*_{ij}(x,y)$ are derivatives of $U^*_{ij}(x,y)$ and $T^*_{ij}(x,y)$, respectively,

$$\begin{aligned} D^*_{ij}(x,y)&=n_k(x)\left[\lambda\,\delta_{ki}\frac{\partial U^*_{lj}(x,y)}{\partial x_l}+G\left(\frac{\partial U^*_{kj}(x,y)}{\partial x_i}+\frac{\partial U^*_{ij}(x,y)}{\partial x_k}\right)\right]\\ &=\frac{1}{8\pi(1-\nu)r^2}\left\{(1-2\nu)\left[\delta_{ij}\frac{r_k n_k(x)}{r}+\frac{r_i n_j(x)-r_j n_i(x)}{r}\right]+3\frac{r_i r_j r_k}{r^3}n_k(x)\right\} \end{aligned} \tag{3a}$$

$$S_{ij}^{*}(x,y) = n_k(x)\left[\lambda\delta_{ki}\frac{\partial T_{lj}^{*}(x,y)}{\partial x_l} + G\left(\frac{\partial T_{kj}^{*}(x,y)}{\partial x_i} + \frac{\partial T_{ij}^{*}(x,y)}{\partial x_k}\right)\right]$$

$$= -\frac{G}{4\pi(1-v)r^3} \tag{3b}$$

$$\left\{\begin{array}{c} 3\frac{\partial r}{\partial n}\left[5r_{,i}r_{,j}r_{,k}n_k(x) - (1-2v)\,r_{,j}n_i(x)\right] + (1-4v)\,n_j(y)\,n_i(x) \\ -3v\left[r_{,i}r_{,j}n_k(y)\,n_k(x) + r_{,k}r_{,j}n_i(y)\,n_k(x) + \delta_{ij}r_{,k}n_k(x)\,\frac{\partial r}{\partial n} + r_{,i}n_j(x)\,\frac{\partial r}{\partial n}\right] \\ -(1-2v)\left[n_i(y)\,n_j(x) + n_k(y)\,n_k(x)\,\delta_{ij} + 3r_{,i}r_{,k}n_j(y)\,n_k(x)\right] \end{array}\right\}$$

with $n_k(x)$ and $n_k(y)$ being the outward normal vectors at point x and y, respectively; λ is the Lame constant.

In order to discretize DBIEs we use collocation method and eight-node quadratic element. Note from Eqs.(1)-(3) that the boundary integrals have weak, strong and hyper singularities. To deal with the strongly- and hyper-singular integrals the concept of finite part integral is used, which requires that the traction and displacement derivatives should be Hölder continuous. In order to satisfy such continuity requirements during the meshing process for discretization of the boundary in a simple and efficient way, we adopt the modeling strategy proposed by Mi and Aliabadi (1992), using discontinuous elements (see Fig. 2(a)) for the crack modeling, edge-discontinuous elements (see Fig. 2(b)) on surfaces approaching the corner or intersecting the crack surface, and continuous elements (see Fig. 2(c)) on all other surfaces. The positioning parameter λ ($0 < \lambda < 1$) of collocation nodes in Fig. 2 stands for the degree of continuity.

In order to achieve the square root displacement variation near the crack front, the quarter point discontinuous elements are generated by simply moving the two midside geometry points of each crack-front element to the quarter position, as shown in Fig. 3. The quarter point technique is only straightly applicable to straight cracks. For curved cracks the crack-front elements with special shape functions may be adopted in the future work.

The stress intensity factors (SIFs) are calculated using the two-point crack opening displacement formulae. The steps are: 1) The relative displacements of two surfaces of the crack, Δu, at the collocation points are obtained by the DBEM analysis; 2) Δu are extrapolated to the position of geometry points; 3) SIFs are given, at

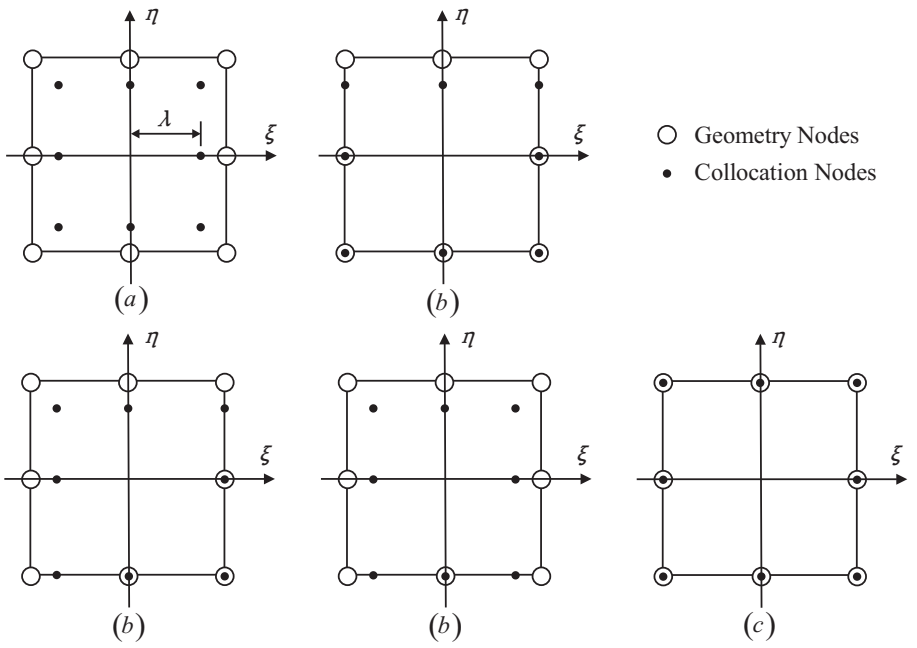

Figure 2: Element Types: (a) discontinuous element (b) edge-discontinuous element (c) continuous element

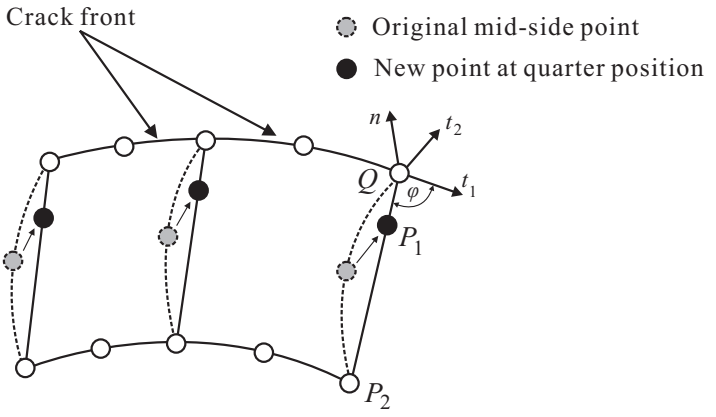

Figure 3: Generation of quarter point element

geometry point Q in Fig.3, by,

$$\begin{aligned} K_I^Q &= \frac{4K_I^{P_1} - K_I^{P_2}}{3} \\ K_{II}^Q &= \frac{4K_{II}^{P_1} - K_{II}^{P_2}}{3} \\ K_{III}^Q &= \frac{4K_{III}^{P_1} - K_{III}^{P_2}}{3} \end{aligned} \tag{4}$$

where

$$\begin{aligned} K_I^P &= \frac{G}{2(1-\nu)\sqrt{\cos\varphi}}\sqrt{\frac{\pi}{2l_{PQ}}}\Delta u_n^P \\ K_{II}^P &= \frac{G}{2(1-\nu)\sqrt{\cos\varphi}}\sqrt{\frac{\pi}{2l_{PQ}}}\Delta u_{t_2}^P \\ K_{III}^P &= \frac{G}{2\sqrt{\cos\varphi}}\sqrt{\frac{\pi}{2l_{PQ}}}\Delta u_{t_1}^P \end{aligned} \tag{5}$$

with l_{PQ} being the distance of P (representing P_1 or P_2) and Q; Δu_n and Δu_t being the normal and tangent components of Δu at P under the local coordinate system defined at Q (see Fig.3).

3 Fast Multipole Dual Boundary Element Method

3.1 Multipole Expansion

A unified form of the multipole expansions of integrals containing $U_{ij}^*(x,y)$ and $T_{ij}^*(x,y)$ for 3-D elasticity has been established in ref. (Wang, Hall, Yu and Yao 2008), adopting a concise expansion formulation proposed in ref. (Yoshida 2001). We extend this form for the multipole expansions of integrals containing $D_{ij}^*(x,y)$ and $S_{ij}^*(x,y)$.

Considering a reference point O close to y and a threshold of $\left|\overrightarrow{Oy}\right| < \left|\overrightarrow{Ox}\right|$ is satisfied, the integrals in Eq. (1a, 1b) can be expanded around O as,

$$\int_{S_0} U_{ij}^*(x,y)\, t_j(y)\, dS(y) = \frac{1}{8\pi G}\sum_{n=0}^{\infty}\sum_{m=-n}^{n}\left(\overline{F_{ij,n,m}^S}\left(\overrightarrow{Ox}\right) M_{j,n,m}^{U1}(O) + \overline{G_{i,n,m}^S}\left(\overrightarrow{Ox}\right) M_{n,m}^{U2}(O)\right) \tag{6a}$$

$$\int_{S_0} T_{ij}^*(x,y)\,u_j(y)\,dS(y) = \frac{1}{8\pi G}\sum_{n=0}^{\infty}\sum_{m=-n}^{n}\left(\overline{F_{ij,n,m}^S}\left(\overrightarrow{Ox}\right)M_{j,n,m}^{T1}(O)+\overline{G_{i,n,m}^S}\left(\overrightarrow{Ox}\right)M_{n,m}^{T2}(O)\right) \quad (6b)$$

$$\int_{S_c^+} T_{ij}^*(x,y)\,\Delta u_j(y)\,dS(y) = \frac{1}{8\pi G}\sum_{n=0}^{\infty}\sum_{m=-n}^{n}\left(\overline{F_{ij,n,m}^S}\left(\overrightarrow{Ox}\right)M_{j,n,m}^{T1,S_c}(O)+\overline{G_{i,n,m}^S}\left(\overrightarrow{Ox}\right)M_{n,m}^{T2,S_c}(O)\right) \quad (6c)$$

where (Yoshida 2001)

$$\begin{aligned} F_{ij,n,m}^S\left(\overrightarrow{Ox}\right) &= \frac{\lambda+3G}{\lambda+2G}\delta_{ij}S_{n,m}\left(\overrightarrow{Ox}\right)-\frac{\lambda+G}{\lambda+2G}\left(\overrightarrow{Ox}\right)_j\frac{\partial}{\partial x_i}S_{n,m}\left(\overrightarrow{Ox}\right) \\ G_{i,n,m}^S\left(\overrightarrow{Ox}\right) &= \frac{\lambda+G}{\lambda+2G}\frac{\partial}{\partial x_i}S_{n,m}\left(\overrightarrow{Ox}\right) \end{aligned} \quad (7)$$

$M_{j,n,m}^{U1}(O), M_{n,m}^{U2}(O), M_{j,n,m}^{T1}(O), M_{n,m}^{T2}(O), M_{j,n,m}^{T1,S_c}(O)$ and $M_{n,m}^{T2,S_c}(O)$ are called multipole moments. Detailed expressions of the multipole moments are given in the Appendix. $S_{n,m}$ are called solid spherical harmonic functions (Yoshida 2001) as defined in the Appendix.

According to the relations of $D_{ij}^*(x,y)/S_{ij}^*(x,y)$ and $U_{ij}^*(x,y)/T_{ij}^*(x,y)$, see Eq.(3), straightforward expansions for the integrals in Eq.(1c) containing $D_{ij}^*(x,y)$ and $S_{ij}^*(x,y)$ give,

$$\begin{aligned} &\int_{S_0} D_{ij}^*(x,y)\,t_j(y)\,dS(y) \\ &= \frac{1}{8\pi G}\sum_{n=0}^{\infty}\sum_{m=-n}^{n} \\ &n_k\left[\lambda\delta_{ki}\frac{\partial\overline{F_{lj,n,m}^S}\left(\overrightarrow{Ox}\right)}{\partial x_l}+G\left(\frac{\partial\overline{F_{kj,n,m}^S}\left(\overrightarrow{Ox}\right)}{\partial x_i}+\frac{\partial\overline{F_{ij,n,m}^S}\left(\overrightarrow{Ox}\right)}{\partial x_k}\right)\right]M_{j,n,m}^{U1}(O) \\ &+\frac{1}{8\pi G}\sum_{n=0}^{\infty}\sum_{m=-n}^{n} \\ &n_k\left[\lambda\delta_{ki}\frac{\partial\overline{G_{l,n,m}^S}\left(\overrightarrow{Ox}\right)}{\partial x_l}+G\left(\frac{\partial\overline{G_{k,n,m}^S}\left(\overrightarrow{Ox}\right)}{\partial x_i}+\frac{\partial\overline{G_{i,n,m}^S}\left(\overrightarrow{Ox}\right)}{\partial x_k}\right)\right]M_{n,m}^{U2}(O) \end{aligned} \quad (8a)$$

$$
\begin{aligned}
&\int_{S_0} S^*_{ij}(x,y)\, u_j(y)\, dS(y) \\
&= \frac{1}{8\pi G} \sum_{n=0}^{\infty} \sum_{m=-n}^{n} \\
&n_k \left[\lambda \delta_{ki} \frac{\partial \overline{F^S_{lj,n,m}}\left(\overrightarrow{Ox}\right)}{\partial x_l} + G \left(\frac{\partial \overline{F^S_{kj,n,m}}\left(\overrightarrow{Ox}\right)}{\partial x_i} + \frac{\partial \overline{F^S_{ij,n,m}}\left(\overrightarrow{Ox}\right)}{\partial x_k} \right) \right] M^{T1}_{j,n,m}(O) \\
&+ \frac{1}{8\pi G} \sum_{n=0}^{\infty} \sum_{m=-n}^{n} \\
&n_k \left[\lambda \delta_{ki} \frac{\partial \overline{G^S_{l,n,m}}\left(\overrightarrow{Ox}\right)}{\partial x_l} + G \left(\frac{\partial \overline{G^S_{k,n,m}}\left(\overrightarrow{Ox}\right)}{\partial x_i} + \frac{\partial \overline{G^S_{i,n,m}}\left(\overrightarrow{Ox}\right)}{\partial x_k} \right) \right] M^{T2}_{n,m}(O)
\end{aligned}
\tag{8b}
$$

$$
\begin{aligned}
&\int_{S_c^+} S^*_{ij}(x,y)\, \Delta u_j(y)\, dS(y) \\
&= \frac{1}{8\pi G} \sum_{n=0}^{\infty} \sum_{m=-n}^{n} \\
&n_k \left[\lambda \delta_{ki} \frac{\partial \overline{F^S_{lj,n,m}}\left(\overrightarrow{Ox}\right)}{\partial x_l} + G \left(\frac{\partial \overline{F^S_{kj,n,m}}\left(\overrightarrow{Ox}\right)}{\partial x_i} + \frac{\partial \overline{F^S_{ij,n,m}}\left(\overrightarrow{Ox}\right)}{\partial x_k} \right) \right] M^{T1,S_c}_{j,n,m}(O) \\
&+ \frac{1}{8\pi G} \sum_{n=0}^{\infty} \sum_{m=-n}^{n} \\
&n_k \left[\lambda \delta_{ki} \frac{\partial \overline{G^S_{l,n,m}}\left(\overrightarrow{Ox}\right)}{\partial x_l} + G \left(\frac{\partial \overline{G^S_{k,n,m}}\left(\overrightarrow{Ox}\right)}{\partial x_i} + \frac{\partial \overline{G^S_{i,n,m}}\left(\overrightarrow{Ox}\right)}{\partial x_k} \right) \right] M^{T2,S_c}_{n,m}(O)
\end{aligned}
\tag{8c}
$$

The essence of Eq.(8) is that the multipole moments of $U^*_{ij}(x,y)$ and $T^*_{ij}(x,y)$ are repeatedly used for the evaluations of the integrals of $D^*_{ij}(x,y)$ and $S^*_{ij}(x,y)$. Therefore, direct expansions of $D^*_{ij}(x,y)$ and $S^*_{ij}(x,y)$ are avoided. Notice that except for the upper index (U, T or T, S_c) for the multipole moments, the multipole expansion formulas for all integrals, at any boundary integral equation in Eq.(1), are unified. This implies that other expansion and translation operator formulas are also unified for all integrals at any boundary integral equation if they are derived using the multipole expansions. Hence we omit the difference in the upper index and use $M^1_{j,n,m}(O)$ and $M^2_{n,m}(O)$ instead of the original six coefficients to carry out the subsequent translation operations.

3.2 Local Expansion

Considering another reference point O' close to x and a threshold of $\left|\overrightarrow{O'x}\right| < \left|\overrightarrow{O'y}\right|$ is satisfied, the integrals in Eq. (1) can be expanded around O' as a 'local expansion' form,

$$\int_{S_0} U^*_{ij}(x,y)\, t_j(y)\, dS(y) = \frac{1}{8\pi G}\sum_{n=0}^{\infty}\sum_{m=-n}^{n}\left(F^R_{ij,n,m}\left(\overrightarrow{O'x}\right) L^{U1}_{j,n,m}(O') + G^R_{i,n,m}\left(\overrightarrow{O'x}\right) L^{U2}_{n,m}(O')\right) \tag{9a}$$

$$\int_{S_0} T^*_{ij}(x,y)\, u_j(y)\, dS(y) = \frac{1}{8\pi G}\sum_{n=0}^{\infty}\sum_{m=-n}^{n}\left(F^R_{ij,n,m}\left(\overrightarrow{O'x}\right) L^{T1}_{j,n,m}(O') + G^R_{i,n,m}\left(\overrightarrow{O'x}\right) L^{T2}_{n,m}(O')\right) \tag{9b}$$

$$\int_{S_c^+} T^*_{ij}(x,y)\, \Delta u_j(y)\, dS(y) = \frac{1}{8\pi G}\sum_{n=0}^{\infty}\sum_{m=-n}^{n}\left(F^R_{ij,n,m}\left(\overrightarrow{O'x}\right) L^{T1,S_c}_{j,n,m}(O') + G^R_{i,n,m}\left(\overrightarrow{O'x}\right) L^{T2,S_c}_{n,m}(O')\right) \tag{9c}$$

$$\begin{aligned}
&\int_{S_0} D^*_{ij}(x,y)\, t_j(y)\, dS(y) \\
&= \frac{1}{8\pi G}\sum_{n=0}^{\infty}\sum_{m=-n}^{n} \\
&n_k\left[\lambda\,\delta_{ki}\frac{\partial F^R_{lj,n,m}\left(\overrightarrow{O'x}\right)}{\partial x_l} + G\left(\frac{\partial F^R_{kj,n,m}\left(\overrightarrow{O'x}\right)}{\partial x_i} + \frac{\partial F^R_{ij,n,m}\left(\overrightarrow{O'x}\right)}{\partial x_k}\right)\right] L^{U1}_{j,n,m}(O') \\
&+ \frac{1}{8\pi G}\sum_{n=0}^{\infty}\sum_{m=-n}^{n} \\
&n_k\left[\lambda\,\delta_{ki}\frac{\partial G^R_{l,n,m}\left(\overrightarrow{O'x}\right)}{\partial x_l} + G\left(\frac{\partial G^R_{k,n,m}\left(\overrightarrow{O'x}\right)}{\partial x_i} + \frac{\partial G^R_{i,n,m}\left(\overrightarrow{O'x}\right)}{\partial x_k}\right)\right] L^{U2}_{n,m}(O')
\end{aligned} \tag{9d}$$

$$
\begin{aligned}
&\int_{S_0} S_{ij}^{*}(x,y)\,u_j(y)\,dS(y) \\
&= \frac{1}{8\pi G}\sum_{n=0}^{\infty}\sum_{m=-n}^{n} \\
&n_k\left[\lambda\,\delta_{ki}\frac{\partial F_{lj,n,m}^{R}\left(\overrightarrow{O'x}\right)}{\partial x_l} + G\left(\frac{\partial F_{kj,n,m}^{R}\left(\overrightarrow{O'x}\right)}{\partial x_i} + \frac{\partial F_{ij,n,m}^{R}\left(\overrightarrow{O'x}\right)}{\partial x_k}\right)\right] L_{j,n,m}^{T1}\left(O'\right) \\
&+ \frac{1}{8\pi G}\sum_{n=0}^{\infty}\sum_{m=-n}^{n} \\
&n_k\left[\lambda\,\delta_{ki}\frac{\partial G_{l,n,m}^{R}\left(\overrightarrow{O'x}\right)}{\partial x_l} + G\left(\frac{\partial G_{k,n,m}^{R}\left(\overrightarrow{O'x}\right)}{\partial x_i} + \frac{\partial G_{i,n,m}^{R}\left(\overrightarrow{O'x}\right)}{\partial x_k}\right)\right] L_{n,m}^{T2}\left(O'\right)
\end{aligned}
\tag{9e}
$$

$$
\begin{aligned}
&\int_{S_c^{+}} S_{ij}^{*}(x,y)\,\Delta u_j(y)\,dS(y) \\
&= \frac{1}{8\pi G}\sum_{n=0}^{\infty}\sum_{m=-n}^{n} \\
&n_k\left[\lambda\,\delta_{ki}\frac{\partial F_{lj,n,m}^{R}\left(\overrightarrow{O'x}\right)}{\partial x_l} + G\left(\frac{\partial F_{kj,n,m}^{R}\left(\overrightarrow{O'x}\right)}{\partial x_i} + \frac{\partial F_{ij,n,m}^{R}\left(\overrightarrow{O'x}\right)}{\partial x_k}\right)\right] L_{j,n,m}^{T1,S_c}\left(O'\right) \\
&+ \frac{1}{8\pi G}\sum_{n=0}^{\infty}\sum_{m=-n}^{n} \\
&n_k\left[\lambda\,\delta_{ki}\frac{\partial G_{l,n,m}^{R}\left(\overrightarrow{O'x}\right)}{\partial x_l} + G\left(\frac{\partial G_{k,n,m}^{R}\left(\overrightarrow{O'x}\right)}{\partial x_i} + \frac{\partial G_{i,n,m}^{R}\left(\overrightarrow{O'x}\right)}{\partial x_k}\right)\right] L_{n,m}^{T2,S_c}\left(O'\right)
\end{aligned}
\tag{9f}
$$

where (Yoshida 2001)

$$
\begin{aligned}
F_{ij,n,m}^{R}\left(\overrightarrow{O'x}\right) &= \frac{\lambda+3G}{\lambda+2G}\delta_{ij}R_{n,m}\left(\overrightarrow{O'x}\right) - \frac{\lambda+G}{\lambda+2G}\left(\overrightarrow{O'x}\right)_j\frac{\partial}{\partial x_i}R_{n,m}\left(\overrightarrow{O'x}\right) \\
G_{i,n,m}^{R}\left(\overrightarrow{O'x}\right) &= \frac{\lambda+G}{\lambda+2G}\frac{\partial}{\partial x_i}R_{n,m}\left(\overrightarrow{O'x}\right)
\end{aligned}
\tag{10}
$$

$R_{n,m}$ are another solid spherical harmonic functions (Yoshida 2001) as defined in the Appendix. $L_{j,n,m}^{U1}(O'), L_{n,m}^{U2}(O'), L_{j,n,m}^{T1}(O'), L_{n,m}^{T2}(O'), L_{j,n,m}^{T1,S_c}(O')$ and $L_{n,m}^{T2,S_c}(O')$

are called local moments. Due to the unified local expansion forms of all integrals at any boundary integral equation of Eq.(1), we omit the difference in the upper index and use $L^1_{j,n,m}(O')$ and $L^2_{n,m}(O')$ instead of the original six local moments. In the FMM framework, the local moments $L^1_{j,n,m}(O')$, $L^2_{n,m}(O')$ are derived by a linear mapping acting on the multipole moments $M^1_{j,n,m}(O)$, $M^2_{n,m}(O)$, instead of being evaluated directly.

3.3 Translation of Multipole and Local Moments

An adaptive tree is constructed based on the geometry information of the boundary elements. This tree is the key structure of the FMM for both operations and data storage. After the multipole moments $M^1_{j,n,m}(O)$ and $M^2_{n,m}(O)$ are collected for each tree leaf centered at O, three kinds of translation operators of the original FMM, namely 1) the multipole to multipole translation (M2M), 2) the multipole to local translation (M2L) and 3) the local to local translation (L2L), are carried out recursively throughout the tree in order to obtain both the multipole moments $M^1_{j,n,m}$, $M^2_{n,m}$ and local moments $L^1_{j,n,m}$, $L^2_{n,m}$ for the tree nodes of various levels. The new version of FMM (Greengard and Rokhlin 1997) can be applied by introducing an 'exponential expansion' and replacing the M2L operator with three new operators, namely 1) the multipole to exponential translation (M2E), 2) exponential to exponential translation (E2E) and 3) exponential to local translation (E2L). With the prefactor greatly reduced, the new FMM performs better in speed than the original version, especially for 3-D problems. Formulas of the translation operators in our work are in the same form as those in Yoshida (2001) for 3-D elastostatics problems.

3.4 Evaluation of Integrals

For each x, the near-field integrals are evaluated directly, and the far-field integrals are evaluated using Eq. (9) by the local moments $L^1_{j,n,m}$, $L^2_{n,m}$ of the tree leaf containing x.

3.5 Iterations

GMRES is used for the iterative solution of the DBEM. At each iterative step, the matrix-vector multiplication is accomplished by the FMM with $O(N)$ operations and storage. Preconditioning techniques are required to make the iteration converge in reasonable speed. In this paper, we consider a left preconditioner matrix with block diagonal forms as in Nishimura, Yoshida and Kobayashi (1999). Each diagonal block is related to one tree leaf and entries of the block are evaluated directly by the collocation nodes contained in the leaf.

4 Numerical results

A C++ code of the new fast multipole DBEM has been developed for the analysis of 3-D general crack problems. In the code, each entry is calculated and stored as an *eight-byte* value. In order to assess the accuracy and efficiency of the proposed method, a number of numerical tests have been carried out, involving the analysis of single and multiple cracks for which analytical solutions exist for comparison. The code runs on a desktop computer with a processor of Intel Core 2 Duo E8400 (3.0GHz) and physical memory of 3GB.

In the following, The Young's modulus and Poisson's ratio are taken to be 250.0 and 0.25, respectively; the positioning parameter λ for discontinuous and edge-discontinuous elements is taken to be 0.67; and in GMRES the relative error is taken to be 10^{-5}. Gaussian quadrature is used for direct evaluations of both the singular and near-field regular integrals. For simplicity, empirical values of the number of integration points are chosen to guarantee the high accuracy: 14×14 Gaussian points are used for singular and hyper-singular integrals at one boundary element based on the finite part integral; three alternative selections are considered for the regular integrals depending on the distance of the source point and the element to be integrated, namely 12×12 Gaussian points are used when $D_{sf} < L^e_{\max}/4$, 8×8 Gaussian points are used when $L^e_{\max}/4 < D_{sf} < 3L^e_{\max}$, and 4×4 Gaussian points are used for the rest, where $L^e_{\max}$ is the largest edge length of the element and D_{sf} is the distance of source point and any geometry point of the element.

4.1 Crack Opening Displacement of a Circular Crack in Infinite Solid under Tension

This test involves the analysis of a circular crack with radius a in an infinite solid under a tensile load σ perpendicular to the crack. The crack is discretized into 300 discontinuous elements with 7,200 DOFs as shown in Fig. 4 (each element is plotted as four corner collocation nodes connected with solid lines in order only to show the effect of discontinuity). The crack opening displacement Δu_n is evaluated using the new fast multipole DBEM. We take 18 terms for the multipole, local and exponential expansions. The calculated normalized crack opening displacement $G\Delta u_n/(a\sigma)$ along the radial direction of the crack is plotted in Fig. 5 and compared with the analytical solution. Good agreement is observed, demonstrating high accuracy of the proposed method and capability of the quarter-point element for modelling square root behavior of the crack opening displacements at crack fronts.

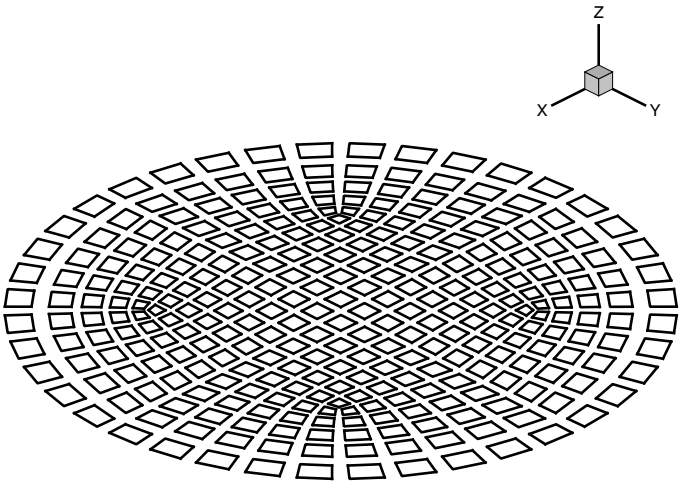

Figure 4: Discontinuous element distribution on the circular crack

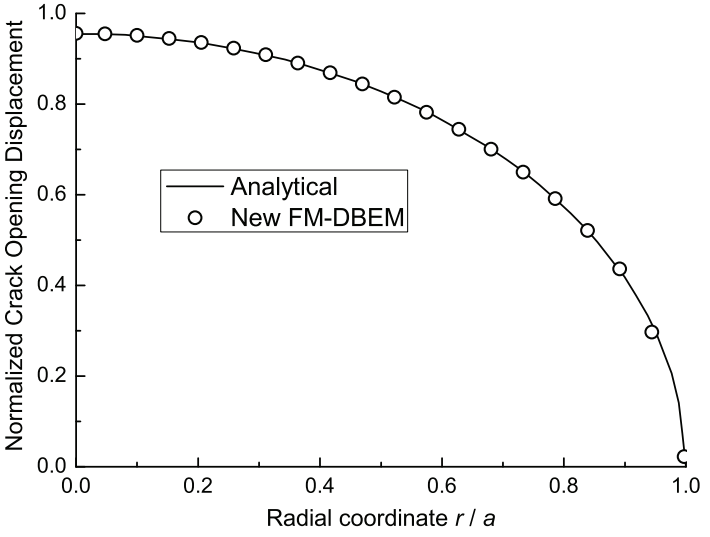

Figure 5: Normalized crack opening displacement versus distance from the crack center

4.2 Stress Intensity Factor of a single crack embedded in a cube under Tension

This test involves the analysis of a cube with edge length L containing an embedded circular crack of radius a. $L / a = 20$. The ends of the cube are subjected to a tensile load σ perpendicular to the crack. Due to the large distance from the center of the crack to the surfaces of the cube, the state of the crack can be treated as a crack in an infinite solid under tension. Hence theoretically the value of the normalized stress intensity factor $K_I / \left(2\sigma\sqrt{a/\pi}\right)$ of the crack is 1.0.

The crack surface is discretized into discontinuous elements, surfaces of the cube are discretized into edge-discontinuous elements at the corners and continuous elements at the rest areas, as shown in Fig. 6. The number of DOFs is 22,368. The stress intensity factor K_I at crack fronts is evaluated using the new fast multipole DBEM. In order to study the influence of the number of terms in the expansion on the accuracy of the solution, we take three selections for the number of multipole, local expansion terms (denoted by p) and exponential expansion terms (denoted by q), namely 1) $p = 10$, $q = 9$; 2) $p = 18$, $q = 18$ and 3) $p = 24$, $q = 27$. The calculated normalized stress intensity factors $K_I / \left(\sigma\sqrt{\pi a}\right)$ of 64 points evenly distributed at the crack front are plotted in Fig. 7. It is shown that all values in Cases 2 ($p = 18$, $q = 18$) and 3 ($p = 24$, $q = 27$) are within 0.5% of the analytical value, and that there is very little difference among these values in the two cases. For Case 1 ($p = 10$, $q = 9$), the relative error ranges from 1% to 3.5%. Therefore, 18 terms in the multipole, local and exponential expansion is large enough to guarantee the accurate solution.

4.3 Stress Intensity Factor of an Elliptical Crack in Infinite Solid under Tension

This test involves the analysis of an elliptical crack with aspect ratio b / a (see Fig. 8) in an infinite solid under a tensile load σ perpendicular to the crack. Three values of aspect ratios are considered, namely $b / a = 1$, 2 and 4. The corresponding meshes with discontinuous elements are shown in Fig. 9. The stress intensity factor K_I along the crack front is evaluated using the new fast multipole DBEM. We take 18 terms for the multipole, local and exponential expansions. The calculated normalized stress intensity factor $K_I / \left(2\sigma\sqrt{a/\pi}\right)$ versus θ defined in Fig. 8 is plotted in Fig. 10 and compared with the analytical solution. Most calculated points agree well with the analytical solution. The only one poor matching at $\theta = 0$ for $b / a = 4$ may be due to the fact that the size of the crack front element at this position is larger than others as in Fig. 9(c), leading to a relative course precision.

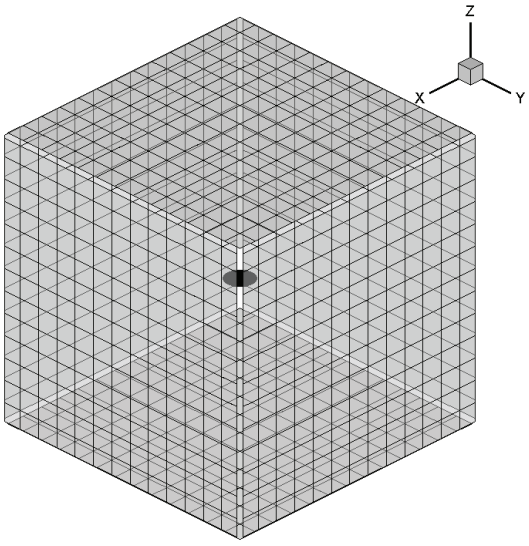

(a)

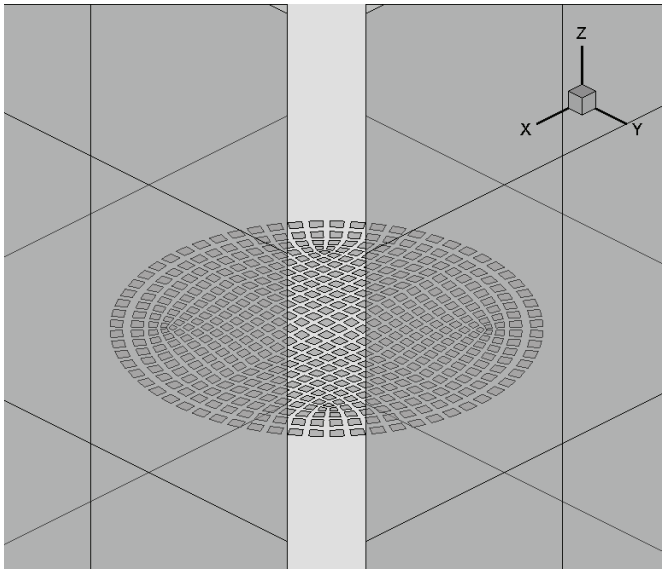

(b)

Figure 6: (a) Global and (b) local translucent view of element distribution on a cube with a circular crack

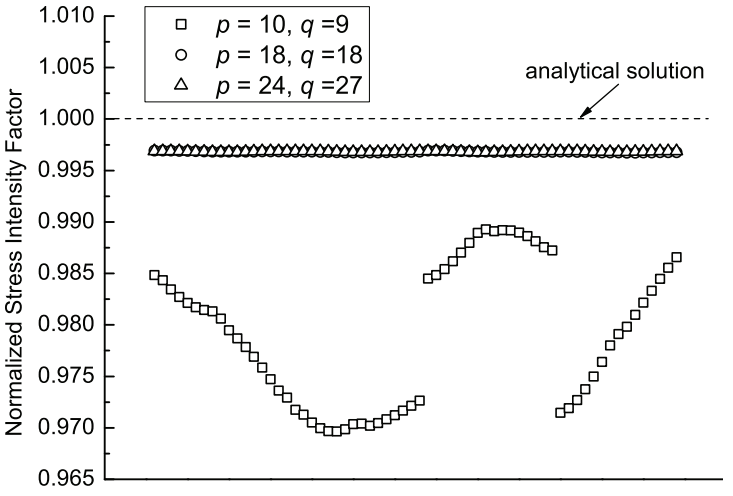

Figure 7: Normalized stress intensity factors $K_I / \left(2\sigma\sqrt{a/\pi}\right)$ of a single crack embedded in a cube

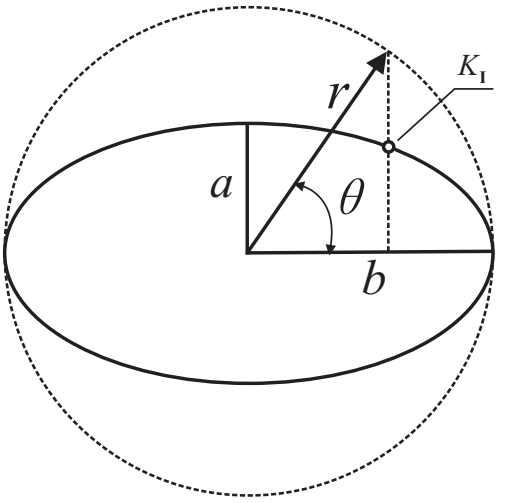

Figure 8: An elliptical crack with aspect ratio *b* / *a*

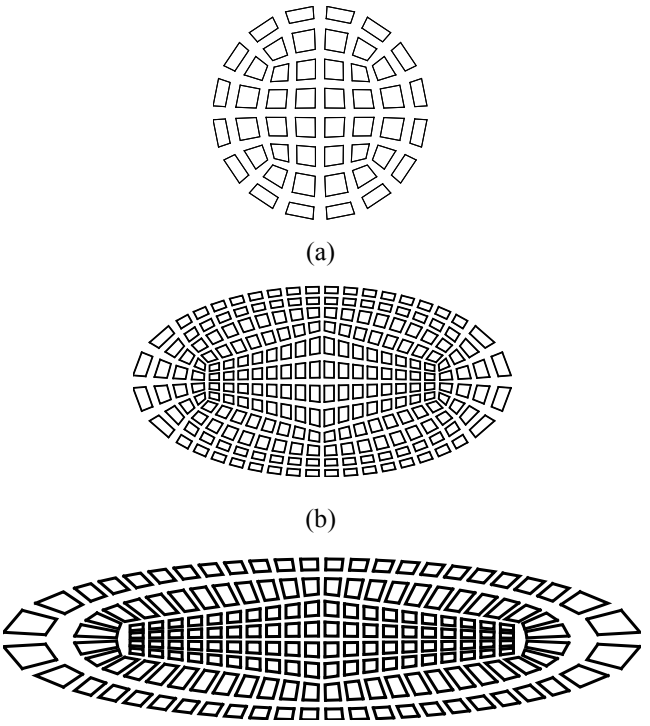

Figure 9: Discontinuous element distribution on the elliptical crack (a) b / a = 1 (b) b / a = 2 (c) b / a = 4

4.4 Stress Intensity Factor of an Edge Crack in a Rectangular Bar under Tension

This test involves the analysis of a rectangular bar of thickness t, width w, total height h, with an edge crack of length a throughout the width, as shown in Fig. 11. t / a = 2, w / a = 3, h / a = 6. The ends of the bar are subjected to a tensile load σ perpendicular to the crack. The state of the deformation in the central area of the bar is approximately regarded as plane strain. For simplicity, both surfaces and crack of the model are discretized into discontinuous elements with 28,800 DOFs as shown in Fig. 12. Besides the quarter point elements generated at the crack tip, we also move the two mid-side geometry points of each free surface element interacting with the crack tip to the quarter position. With this adjustment, we achieve both the $\sqrt{r}$ displacement variation at this area and $\sqrt{1/r}$ stress variation calculated from displacement derivatives. The stress intensity factor K_I along the

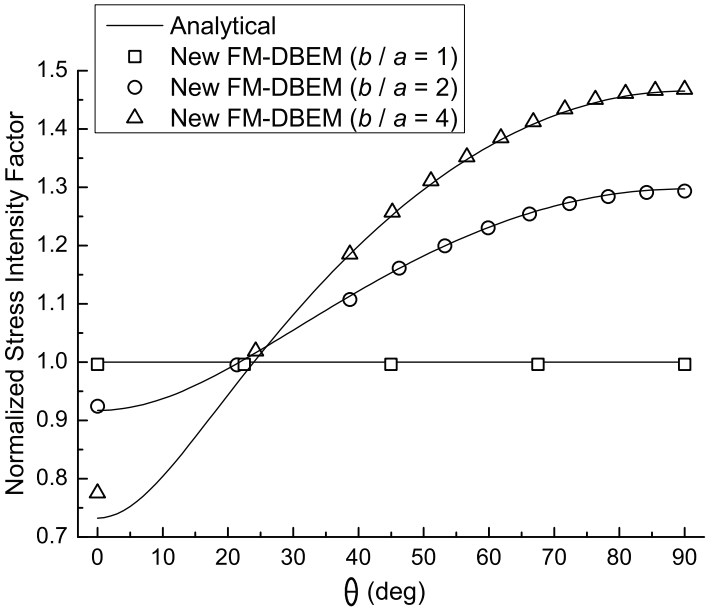

Figure 10: Normalized stress intensity factor $K_I/\left(2\sigma\sqrt{a/\pi}\right)$ versus θ

crack front is evaluated using the new fast multipole DBEM. We take 18 terms for the multipole, local and exponential expansions. The calculated normalized stress intensity factor $K_I/\left(\sigma\sqrt{\pi a}\right)$ is plotted in Fig. 13 and compared with the analytical plane strain solution. The numerical result at the center of the bar is within 2% of the plane strain value.

Stresses on free surfaces are postprocessed using displacement derivatives. The calculated normalized radial stresses $\sigma_{rr}\left(\sqrt{a}/K_I\right)$ (see Fig. 11) near the crack tip ($r \ll a$) are 1.24 at $r/a = 0.0625, \theta = 0$ and 1.65 at $r/a = 0.0625, \theta = \pi/2$, within 23% and 3% of the plane stress values 1.59 and 1.69 from Eq. (11), respectively. It is shown that surface stresses calculated from displacement derivatives have relatively poor accuracy compared with the stress intensity factor.

$$\sigma_{rr} = \frac{K_I}{4\sqrt{2\pi r}}\left(5\cos\frac{\theta}{2} - \cos\frac{3}{2}\theta\right) \Rightarrow \sigma_{rr}\left(\sqrt{a}/K_I\right) = \frac{1}{4\sqrt{2\pi}}\sqrt{\frac{a}{r}}\left(5\cos\frac{\theta}{2} - \cos\frac{3}{2}\theta\right), \quad r \ll a \quad (11)$$

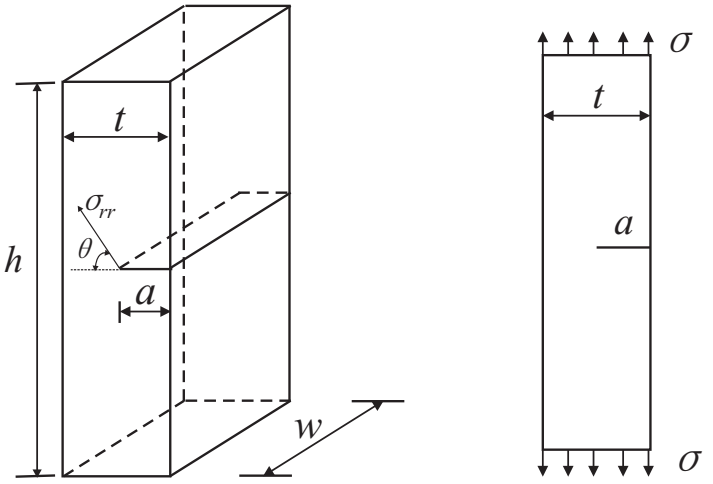

Figure 11: A rectangular bar with an edge crack throughout the width

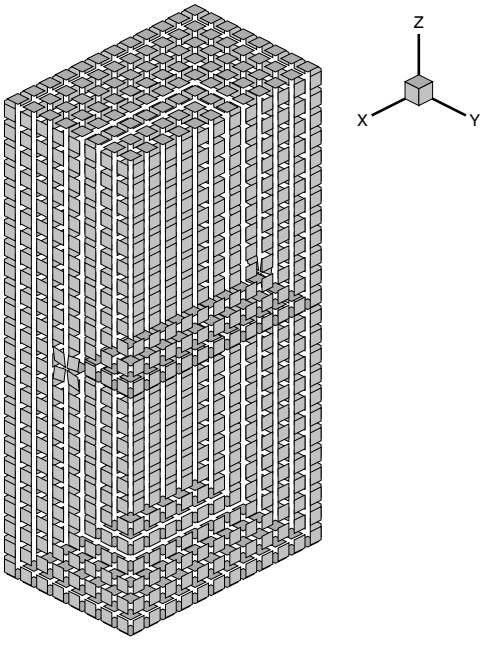

Figure 12: Discontinuous element distribution on the edge-cracked bar

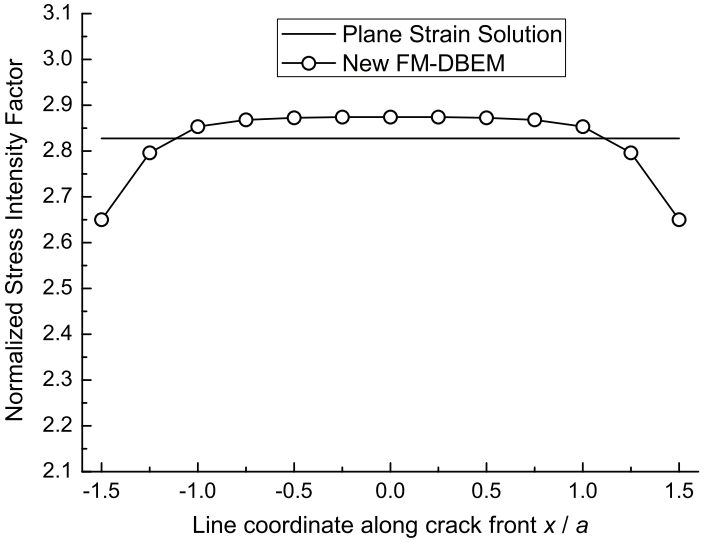

Figure 13: Normalized stress intensity factor $K_I/\left(\sigma\sqrt{\pi a}\right)$ along the crack front

4.5 Stress Intensity Factors of an array of cracks embedded in a cube under Tension

This test involves the analysis of a cube of edge length L containing an array of $5 \times 5 \times 5\,(125)$ embedded circular cracks of the same radius a. $L / a = 60$. The centers of these cracks are located regularly at the interval of $10a$ in all the coordinate directions. All cracks are in the same orientation, with normal vectors parallel to Z axis. The ends of the cube are subjected to a tensile load σ perpendicular to the cracks. Due to the large distance from the center of one crack to others and to the surfaces of the cube, the state of each crack can be treated as a crack in an infinite solid under tension. Hence theoretically the values of the normalized stress intensity factors $K_I/\left(2\sigma\sqrt{a/\pi}\right)$ of all cracks are the same to be 1.0.

All crack surfaces are discretized into discontinuous elements, surfaces of the cube are discretized into edge-discontinuous elements at the corners and continuous elements at the rest areas, as shown in Fig. 14. The number of DOFs reaches up to 167,058. The stress intensity factor K_I at crack fronts is evaluated using the new fast multipole DBEM. We take 18 terms for the multipole, local and exponential expansions. A local view of the crack opening displacements is given in Fig. 15. The calculated normalized stress intensity factors $K_I/\left(\sigma\sqrt{\pi a}\right)$ of 2,000 points at crack fronts (16 points evenly distributed at each crack front) are plotted in Fig.

16. It is shown that most values are within 1% of the analytical value, and that the biggest error is within 1.4%. The results clearly demonstrate accuracy of the proposed method for large-scale problems.

4.6 Memory Requirement and Solution Time of New Fast Multipole DBEM

In order to evaluate the performance of the proposed method in both memory consumption and solution time, a comparison was made on the computational efficiency between the fast multipole DBEM and several other algorithms including the LAPACK-based standard Gaussian elimination and the fully-pivoted ACA. The codes of the latter two solvers are written via C++ in authors' group. The fully-pivoted ACA is chosen instead of the partially-pivoted version for comparison because the key factor for large-scale BEM solutions is memory rather than speed, and that the fully-pivoted version consumes similar memory to the partially-pivoted version but is much easier than the latter one to be implemented for vector problems. The problems to be solved are an array of $n \times n \times n$ cracks in an infinite solid under tension, with n ranging from 1 to 6. The largest model ($6 \times 6 \times 6$ cracks) has 248,832 DOFs. For the new fast multipole DBEM we take 10 terms for the multipole, local expansions and 9 terms for the exponential expansions. A global view of the crack opening displacements of the largest model is given in Fig. 17.

The memory requirements of various solvers versus the number of DOFs are plotted in Fig. 18. It is shown that the new fast multipole DBEM consumes the least memory among the three solvers. Gaussian elimination requires around 25MB at DOF=1152 which is around twice the theoretical value of $O\left(N^2\right)$ storage for the coefficient matrix ($1152^2 \times 8/1024^2 = 10MB$). This is due to the additional memory requirement for the common variables defined in authors' coding that help enhance the integration efficiency. The fast multipole DBEM has a perfect $O(N)$ scale except that the value at DOF=1152 beyond this linear trend. This is also due to the common variables which consume comparable memory with the FMM tree structure at such small scales but are neglectable at large scales. Due to the memory limit of a common PC (e.g., 1GB), capabilities of the three solvers are such that around 10,000 DOFs by Gaussian elimination, less than 100,000 DOFs by ACA and several hundred thousands DOFs by the new fast multipole DBEM. Hence the new fast multipole DBEM is more competitive than other two solvers for 3-D large-scale crack problems.

Solution time of various solvers versus the number of DOFs is plotted in Fig. 19. According to the trends, it is indicated that the break-even points will be at $DOF \approx 10000$ for Gaussian elimination / new fast multipole DBEM and at $DOF \approx 35000$ for fully-pivoted ACA / new fast multipole DBEM. For larger scales, the new fast multipole DBEM is the fastest.

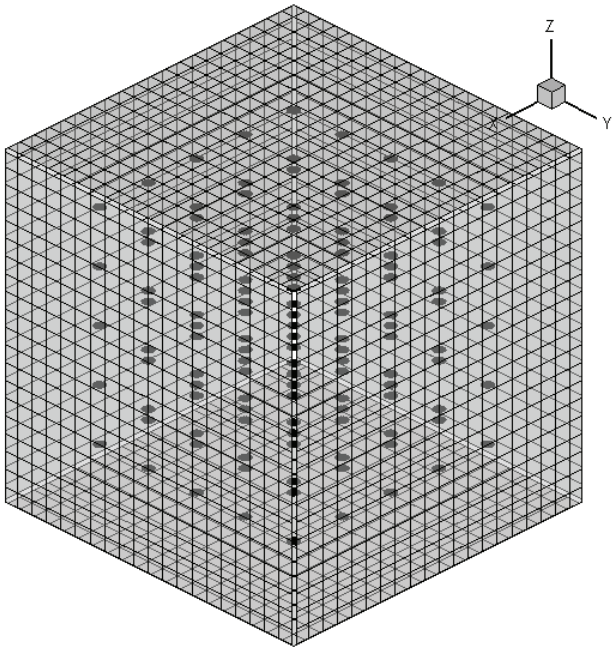

(a)

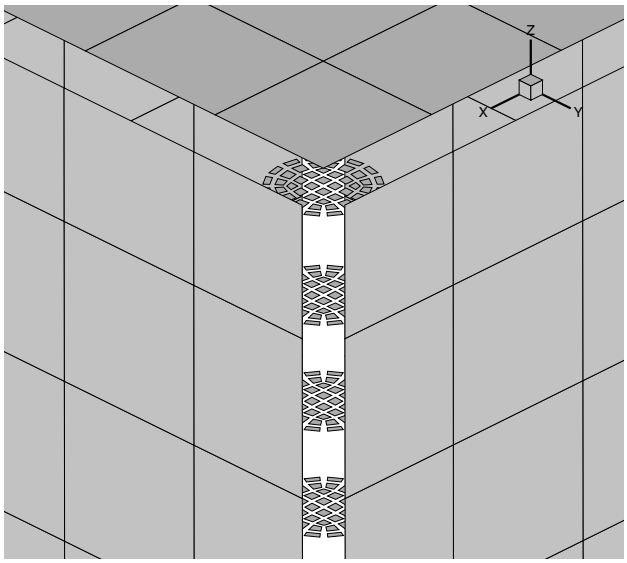

(b)

Figure 14: (a) Global translucent view and (b) local view of element distribution on a cube containing an array of $5 \times 5 \times 5\,(= 125)$ circular cracks

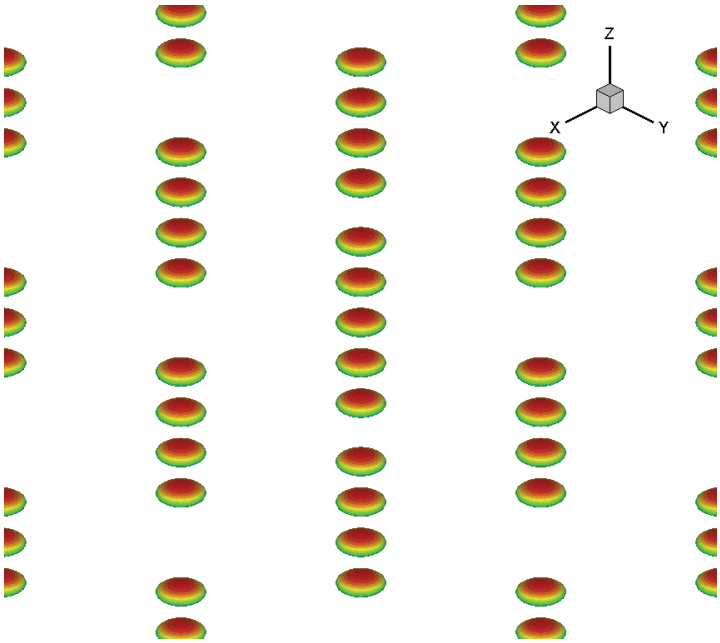

Figure 15: Local view of crack opening displacements

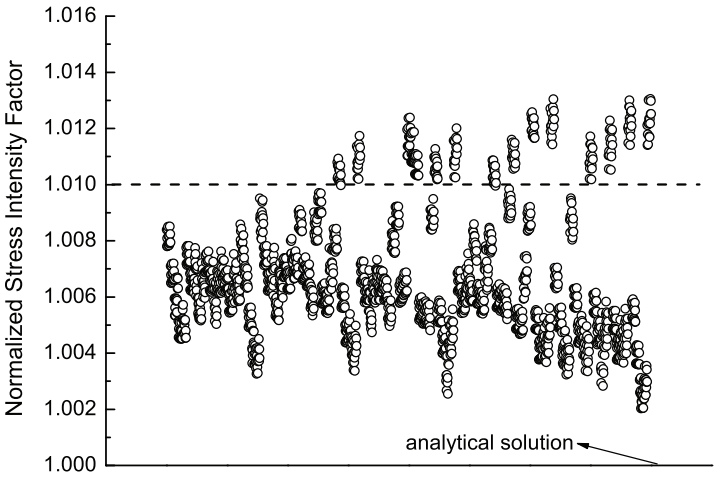

Figure 16: Normalized stress intensity factors $K_I/\left(2\sigma\sqrt{a/\pi}\right)$ of $5\times5\times5\,(=125)$ circular cracks

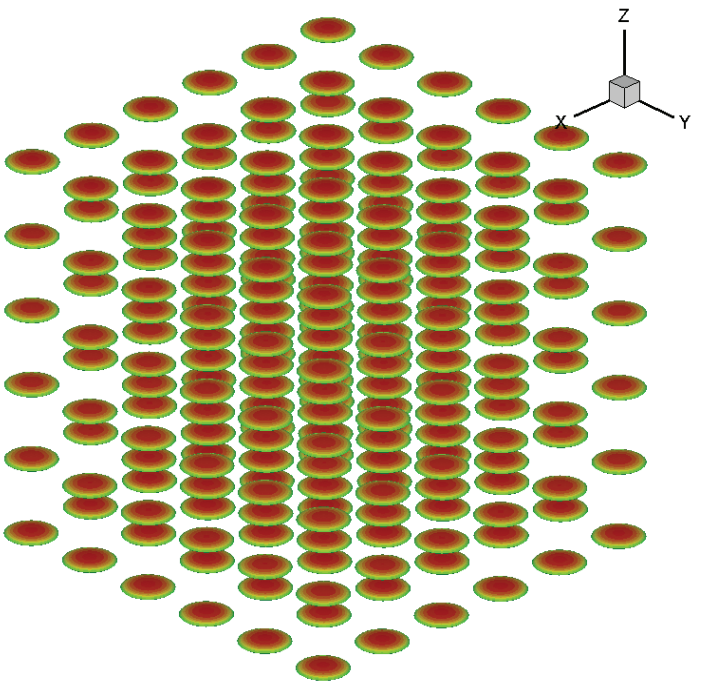

Figure 17: Global view of crack opening displacements of $6 \times 6 \times 6$ cracks

5 Conclusions

A fast boundary element solver has been developed for the analysis of three-dimensional general crack problems. A dual boundary integral equation formulation was used to model the embedded or edge cracked structures in an efficient way. The new fast multipole method was applied to the solution of the discretized DBIE so that large-scale modeling of crack problems can be carried out in a personal desktop computer. In order to make the multipole moments of the integrals containing kernels of various singularities collected and translated in a unified form, a multipole expansion formulation was derived for the hyper-singular integral. Several numerical tests were presented to demonstrate accuracy of the proposed method and its capability for the solution of large-scale 3-D crack problems.

Acknowledgement: Financial support for the project from the National Natural Science Foundation of China, under grant No. 10602029 is gratefully acknowledged. The authors would also like to thank the Royal Academy of Engineering.

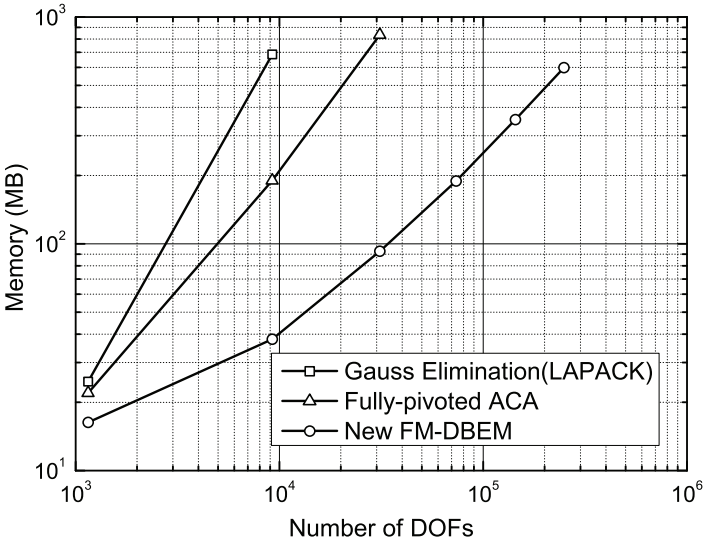

Figure 18: Memory requirement versus DOFs

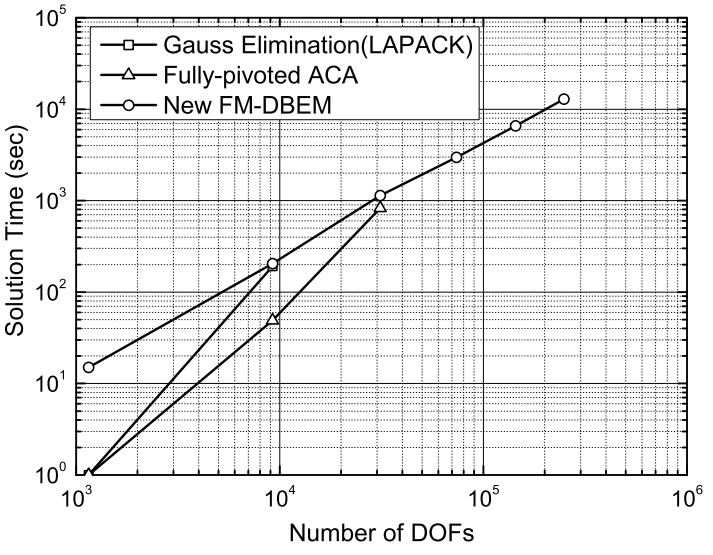

Figure 19: Solution time versus DOFs

Appendix

In this section, we give a summary of detailed expressions of the multipole moments in Eq. (6). The solid spherical harmonic function and their derivatives are defined accordingly, which can be found in Yoshida (2001).

Multipole moments:

$$M_{j,n,m}^{U1}(O) = \int_{S_0} R_{n,m}\left(\overrightarrow{Oy}\right) t_j(y)\, dS(y) \tag{A1}$$

$$M_{n,m}^{U2}(O) = \int_{S_0} \left(\overrightarrow{Oy}\right)_j R_{n,m}\left(\overrightarrow{Oy}\right) t_j(y)\, dS(y) \tag{A2}$$

$$\begin{aligned} M_{j,n,m}^{T1}(O) =& \lambda \int_{S_0} \frac{\partial R_{n,m}\left(\overrightarrow{Oy}\right)}{\partial y_j} n_k(y)\, u_k(y)\, dS(y) \\ &+ G \int_{S_0} \frac{\partial R_{n,m}\left(\overrightarrow{Oy}\right)}{\partial y_k} n_j(y)\, u_k(y)\, dS(y) \\ &+ G \int_{S_0} \frac{\partial R_{n,m}\left(\overrightarrow{Oy}\right)}{\partial y_k} n_k(y)\, u_j(y)\, dS(y) \end{aligned} \tag{A3}$$

$$\begin{aligned} & M_{n,m}^{T2}(O) = \\ & (3\lambda + 2G) \int_{S_0} R_{n,m}\left(\overrightarrow{Oy}\right) n_k(y)\, u_k(y)\, dS(y) \\ & + \lambda \int_{S_0} \left(\overrightarrow{Oy}\right)_j \frac{\partial R_{n,m}\left(\overrightarrow{Oy}\right)}{\partial y_j} n_k(y)\, u_k(y)\, dS(y) \\ & + G \int_{S_0} \left[\left(\overrightarrow{Oy}\right)_j \frac{\partial R_{n,m}\left(\overrightarrow{Oy}\right)}{\partial y_k} + \left(\overrightarrow{Oy}\right)_k \frac{\partial R_{n,m}\left(\overrightarrow{Oy}\right)}{\partial y_j} \right] n_j(y)\, u_k(y)\, dS(y) \end{aligned} \tag{A4}$$

$$\begin{aligned} M_{j,n,m}^{T1,S_c}(O) =& \lambda \int_{S_c^+} \frac{\partial R_{n,m}\left(\overrightarrow{Oy}\right)}{\partial y_j} n_k(y)\, \Delta u_k(y)\, dS(y) \\ &+ G \int_{S_c^+} \frac{\partial R_{n,m}\left(\overrightarrow{Oy}\right)}{\partial y_k} n_j(y)\, \Delta u_k(y)\, dS(y) \\ &+ G \int_{S_c^+} \frac{\partial R_{n,m}\left(\overrightarrow{Oy}\right)}{\partial y_k} n_k(y)\, \Delta u_j(y)\, dS(y) \end{aligned} \tag{A5}$$

$$
\begin{aligned}
&M_{n,m}^{T2,S_c}(O) = \\
&(3\lambda+2G)\int_{S_c^+} R_{n,m}\left(\overrightarrow{Oy}\right) n_k(y)\,\Delta u_k(y)\,dS(y) \\
&+\lambda\int_{S_c^+}\left(\overrightarrow{Oy}\right)_j \frac{\partial R_{n,m}\left(\overrightarrow{Oy}\right)}{\partial y_j} n_k(y)\,\Delta u_k(y)\,dS(y) \\
&+G\int_{S_c^+}\left[\left(\overrightarrow{Oy}\right)_j \frac{\partial R_{n,m}\left(\overrightarrow{Oy}\right)}{\partial y_k} + \left(\overrightarrow{Oy}\right)_k \frac{\partial R_{n,m}\left(\overrightarrow{Oy}\right)}{\partial y_j}\right] n_j(y)\,\Delta u_k(y)\,dS(y)
\end{aligned}
\tag{A6}
$$

Solid spherical harmonic functions and derivatives:

$$
R_{n,m}\left(\overrightarrow{Oy}\right) = \frac{1}{(n+m)!} P_n^m(\cos\theta)\, e^{im\phi} r^n \tag{A7}
$$

$$
S_{n,m}\left(\overrightarrow{Oy}\right) = (n-m)!\, P_n^m(\cos\theta)\, e^{im\phi} \frac{1}{r^{n+1}} \tag{A8}
$$

$\{r,\theta,\phi\}$ are the spherical coordinates of vector $\overrightarrow{Oy}$, P_n^m is the associated Legendre function.

$$
\begin{aligned}
\frac{\partial}{\partial y_1} R_{n,m}\left(\overrightarrow{Oy}\right) &= \frac{1}{2}\left[R_{n-1,m-1}\left(\overrightarrow{Oy}\right) - R_{n-1,m+1}\left(\overrightarrow{Oy}\right)\right] \\
\frac{\partial}{\partial y_2} R_{n,m}\left(\overrightarrow{Oy}\right) &= \frac{i}{2}\left[R_{n-1,m-1}\left(\overrightarrow{Oy}\right) + R_{n-1,m+1}\left(\overrightarrow{Oy}\right)\right] \\
\frac{\partial}{\partial y_3} R_{n,m}\left(\overrightarrow{Oy}\right) &= R_{n-1,m}\left(\overrightarrow{Oy}\right)
\end{aligned}
\tag{A9}
$$

$$
\begin{aligned}
\frac{\partial}{\partial y_1} S_{n,m}\left(\overrightarrow{Oy}\right) &= \frac{1}{2}\left[S_{n+1,m-1}\left(\overrightarrow{Oy}\right) - S_{n+1,m+1}\left(\overrightarrow{Oy}\right)\right] \\
\frac{\partial}{\partial y_2} S_{n,m}\left(\overrightarrow{Oy}\right) &= \frac{i}{2}\left[S_{n+1,m-1}\left(\overrightarrow{Oy}\right) + S_{n+1,m+1}\left(\overrightarrow{Oy}\right)\right] \\
\frac{\partial}{\partial y_3} S_{n,m}\left(\overrightarrow{Oy}\right) &= -S_{n+1,m}\left(\overrightarrow{Oy}\right)
\end{aligned}
\tag{A10}
$$

References

Albuquerque, E. L.; Sollero, P.; Aliabadi, M. H. (2004): Dual boundary element method for anisotropic dynamic fracture mechanics. *Int J Numer Methods Engng*, vol. 59, pp. 1187–1205.

Aliabadi, M. H. (1997): A new generation of boundary element methods in fracture mechanics. *Int J Fracture*, vol. 86, pp. 91–125.

Bebendorf, M.; Rjasanow, S. (2003): Adaptive low-rank approximation of collocation matrices. *Computing*, vol. 70, pp. 1–24.

Benedetti, I.; Aliabadi, M. H.; Davì, G. (2008): A fast 3D dual boundary element method based on hierarchical matrices. *Int J Solids and Structures*, vol. 45, pp. 2355–2376.

Benedetti, I.; Milazzo, A.; Aliabadi, M. H. (2009): A fast dual boundary element method for 3D anisotropic crack problems. *Int J Numer Methods Engng*, vol. 80, pp. 1356–1378.

Benedetti, I.; Aliabadi, M. H. (2010): A fast hierarchical dual boundary element method for three-dimensional elastodynamic crack problems. *Int J Numer Methods Engng*, vol. 84, pp. 1038–1067.

Blandford, G. E.; Ingraffea, A. R.; Liggett, J. A. (1981): Two-dimensional stress intensity factor computations using the boundary element method. *Int J Numer Methods Engng*, vol. 17, no. 3, pp. 387–404.

Brancati, A.; Aliabadi, M. H.; Benedetti, I. (2009): Hierarchical adaptive cross approximation GMRES technique for solution of acoustic problems using the boundary element method. *CMES: Computer Modeling & Engineering Sciences*, vol. 43, pp. 149–172.

Brunner, D.; Junge, M.; Rapp, P.; Bebendorf, M.; Gaul, L. (2010): Comparison of the fast multipole method with hierarchical matrices for the Helmholtz-BEM. *CMES: Computer Modeling & Engineering Sciences*, vol. 58, pp. 131–158.

Buchau, A.; Rucker, W.; Rain, O.; Rischmüller, V.; Kurz, S.; Rjasanow, S. (2003): Comparison between different approaches for fast and efficient 3-D BEM computations. *IEEE T Magn*, vol. 39, pp. 1107–1110.

Burczynski, T.; Beluch, W. (2001): The identification of cracks using boundary elements and evolutionary algorithms. *Engrg Anal Boundary Elements*, vol. 25, pp. 313–322.

Chao, R. M.; Chen, Y. J.; Lin, F. C. (2001): Determining the unknown traction of a cracked elastic body using the inverse technique with the dual boundary element method. *CMES: Computer Modeling in Engineering & Sciences*, vol. 2, no. 1, pp. 73–85.

Chen, J. T.; Chen, K. H.; Yeih, W.; Shieh, N. C. (1998): Dual boundary element analysis for cracked bars under torsion. *Engineering Computations*, vol.15, no. 6-7, pp. 732–749.

Chen, W. H.; Chen, T. C. (1995): An efficient dual boundary-element technique for a 2-dimensional fracture problem with multiple cracks. *Int J Numer Methods Engng*, vol. 38, no. 10, pp. 1739–1756.

Cisilino, A. P.; Aliabadi, M. H. (1997): Three-dimensional BEM analysis for fatigue crack growth in welded components. *Int J Pres Ves & Piping*, vol. 70, pp. 135–144.

Cisilino, A. P.; Aliabadi, M. H. (2004): Dual boundary element assessment of three-dimensional fatigue crack growth. *Engrg Anal Boundary Elements*, vol. 28, no. 9, pp. 1157–1173.

Cruse, T. A. (1996): BIE fracture mechanics analysis: 25 years of developments. *Comput Mech*, vol. 18, no. 1, pp. 1–11.

Englund, J. (2006): Efficient algorithm for edge cracked geometries. *Int J Numer Methods Engng*, vol. 66, pp. 1791–1816.

Fu, Y. H.; Klimkowski, K. J.; Rodin, G. J.; Berger, E.; Browne, J. C.; Singer, J. K.; Geijn, R. A.; Vernaganti, K. S. (1998): A fast solution method for three-dimensional many-particle problems of linear elasticity. *Int J Numer Methods Engng*, vol. 42, pp. 1215–1229.

Greengard, L.; Rokhlin, V. (1997): A new version of the fast multipole method for the Laplace equation in three dimensions. *Acta Numer.,* vol. 6, pp. 229–270.

Helsing, J. (1999): Fast and accurate numerical solution to an elastostatic problem involving ten thousand randomly oriented cracks. *Int J Fracture*, vol. 100, no. 4, pp. 321–327.

Helsing, J.; Jonsson, A. (2002): Stress calculations on multiply connected domains. *J Comput Phys*, vol. 176, pp. 456–482.

Kebir, H.; Roelandt, J. M.; Chambon, L. (2006): Dual boundary element method modelling of aircraft structural joints with multiple site damage. *Engng Fracture Mech*, vol. 73, no. 4, pp. 418–434.

Kolk, K.; Weber, W.; Kuhn, G. (2005): Investigation of 3D crack propagation problems via fast BEM formulations. *Comput Mech*, vol. 37, pp. 32–40.

Kolk, K.; Kuhn, G. (2006): The advanced simulation of fatigue crack growth in complex 3D structures. *Archive of Applied Mechanics*, vol. 76, no. 11-12, 699–709.

Lai, Y. S.; Rodin, G. J. (2003): Fast boundary element method for three-dimensional solids containing many cracks. *Engrg Anal Boundary Elements*, vol. 27, pp. 845–852.

Liu, Y. J.; Nishimura, N.; Otani, Y.; Takahashi, T.; Chen, X. L.; Munakata, H. (2005): A fast boundary element method for the analysis of fiber-reinforced composites based on a rigid-inclusion model. *J Appl Mech*, vol. 72, no. 1, pp. 115–128.

Liu, Y. J. (2006): A new fast multipole boundary element method for solving large-

scale two-dimensional elastostatic problems. *Int J Numer Methods Engng*, vol. 65, no. 6, pp. 863–881.

Liu, Y. J. (2008): A fast multipole boundary element method for 2D multi-domain elastostatic problems based on a dual BIE formulation, *Comp Mech*, vol. 42, no. 5, pp. 761–773.

Mi, Y.; Aliabadi, M. H. (1992): Dual boundary element method for three-dimensional fracture mechanics analysis. *Engrg Anal Boundary Elements*, vol. 10, pp. 161–171.

Mi, Y.; Aliabadi, M. H. (1994): Three-dimensional crack growth simulation using BEM. *Comput Struct*, vol. 52, no. 5, pp. 871–878.

Nishimura, N.; Yoshida, K.; Kobayashi, S. (1999): A fast multipole boundary integral equation method for crack problems in 3D. *Engrg Anal Boundary Elements*, vol. 23, pp. 97–105.

Nishimura, N. (2002): Fast multipole accelerated boundary integral equation methods. *Appl Mech Rev*, vol. 55, no. 4, pp. 299–324.

Partheymüller, P.; Haas, M.; Kuhn, G. (2000): Comparison of the basic and the discontinuity formulation of the 3D-dual boundary element method. *Engrg Anal Boundary Elements*, vol. 24, pp. 777–788.

Popov, V.; Power, H. (2001): An O(N) Taylor series multipole boundary element method for three-dimensional elasticity problems. *Engrg Anal Boundary Elements*, vol. 25, pp. 7–18.

Portela, A.; Aliabadi, M. H.; Rooke, D. P. (1992): The dual boundary element method: effective implementation for crack problems. *Int J Numer Methods Engng*, vol. 33, pp. 1269–1287.

Portela, A.; Aliabadi, M. H.; Rooke, D. P. (1993): Dual boundary element incremental analysis of crack propagation. *Comput Struct*, vol. 46, no. 2, pp. 237–247.

Purbolaksono, I.; Aliabadi, M. H. (2005): Dual boundary element method for instability analysis of cracked plates. *CMES: Computer Modeling in Engineering & Sciences*, vol. 8, no. 1, pp. 73–90.

Rokhlin, V. (1985): Rapid solution of integral equations of classical potential theory. *J Comp Phys*, vol. 60, pp. 187–207.

Salgado, N. K.; Aliabadi, M. H. (1996): The application of the dual boundary element method to the analysis of cracked stiffened panels. *Engng Fracture Mech*, vol. 54, no. 1, pp. 91–105.

Sanz, J. A.; Bonnet, M.; Dominguez, J. (2008): Fast multipole method applied to 3-D frequency domain elastodynamics. *Engrg Anal Boundary Elements*, vol. 32, pp. 787–795.

Snyder, M. D.; Cruse, T. A. (1975): Boundary-integral equation analysis of cracked anisotropic plates. *Int J Fracture*, vol. 11, pp. 315–328.

Takahashi, T.; Nishimura, N.; Kobayashi, S. (2003): A fast BIEM for three-dimensional elastodynamics in time domain. *Engrg Anal Boundary Elements*, vol. 27, pp. 803–823.

Wang, H. T.; Yao, Z. H. (2005): A new fast multipole boundary element method for large scale analysis of mechanical properties in 3-D particle-reinforced composites. *CMES: Computer Modeling in Engineering & Science*, vol. 7, no. 1, pp. 85–95.

Wang, H. T.; Hall, G.; Yu, S. Y.; Yao, Z. H. (2008): Numerical simulation of graphite properties using X-ray tomography and fast multipole boundary element method. *CMES: Computer Modeling in Engineering & Sciences*, vol. 37, no. 2, pp. 153–174.

Wang, H. T.; Yao, Z. H. (2008): A rigid-fiber-based boundary element model for strength simulation of carbon nanotube reinforced composites. *CMES: Computer Modeling in Engineering & Sciences*, vol. 29, no. 1, pp. 1–13.

Wang, P. B.; Yao, Z. H. (2006): Fast multipole DBEM analysis of fatigue crack growth. *Comput Mech*, vol. 38, no. 3, pp. 223–233.

Weaver, J. (1977): Three-dimensional crack analysis. *Int J Solids and Structures*, vol. 13, no. 4, pp. 321–330.

Weber, W.; Kolk, K.; Kuhn, G. (2009): Acceleration of 3D crack propagation simulation by the utilization of fast BEM-techniques. *Engrg Anal Boundary Elements*, vol. 33, no. 8-9, pp. 1005–1015.

Wilde, A. J.; Aliabadi, M. H. (1999): A 3-D dual BEM formulation for the analysis of crack growth. *Comput Mech*, vol. 23, pp. 250–257.

Yoshida, K.; Nishimura, N.; Kobayashi, S. (2001): Application of fast multipole Galerkin boundary integral equation method to elastostatic crack problems in 3D. *Int J Numer Methods Engng*, vol. 50, pp. 525–547.

Yoshida, K. (2001): Applications of fast multipole method to boundary integral equation method. *Ph.D. dissertation, Department of Global Environment Engineering, Kyoto University.*

Young, A. (1996): A single-domain boundary element method for 3-D elastostatic crack analysis using continuous elements. *Int J Numer Methods Engng*, vol. 39, pp. 1265–1293.